AIAA JOURNAL
Vol. 46, No. 3, March 2008

Topology Optimization of a Reinforced Wing Box for Enhanced Roll Maneuvers

Alexandra A. Gomes* and Afzal Suleman†
Institute of Mechanical Engineering,
Instituto Superior Técnico, Technical University of Lisbon, 1049-001 Lisbon, Portugal

DOI: 10.2514/1.23028

In this paper, the aileron reversal speed of a wing torsion box is maximized by reinforcing its upper skin. We propose a topology optimization approach using the spectral level set methodology. This is based on the level set methods, which represent the interface describing the reinforcements as the zero level set of a function. According to the proposed methodology, this function is discretized using its Fourier coefficients. These coefficients become the design variables of the optimization problem assigned to define the reinforcing layout. Results show that approximately the same optimal reinforcement layout is obtained from topologically different initial configurations. The two underlying ideas of the present work are to propose the spectral level set methodology as a framework for topology optimization, given its potential for reducing the design space dimension, and, considering the possibilities of new custom-made materials, to readdress the reinforcement perspective in aircraft structures without the weight penalty.

Nomenclature

a_i, b_i	=	problem domain boundaries corresponding to component i of x
a_t	=	χ_t smoothness parameter
a_V	=	χ_V smoothness parameter
a_0	=	lift curve slope
b_t	=	minimum thickness
C	=	positive constant
C_{l_δ}	=	derivative of the rolling moment coefficient of the rigid airplane with respect to δ
$C^{\theta\theta}(y, n)$	=	twist at y produced by a unit moment at η
c	=	wing chord
c_{mAC}	=	local moment coefficient
f	=	generic augmented objective function
$\tilde{f}$	=	generic objective function
g	=	generic inequality constraint
J	=	value of the objective function at the optimum
k	=	element of $\mathbb{Z}^n$
l	=	wing half span
l_1, l_2	=	spanwise aileron boundaries
m	=	arbitrarily large parameter
N	=	square radius
n	=	dimension of the domain of ψ
p_i	=	problem domain period corresponding to component i of x
q_R	=	aileron reversal dynamic pressure
$\mathbb{R}$	=	space of real numbers
S	=	wing planform area
V_{reinf}	=	reinforcing material volume
V_{total}	=	original upper skin volume
χ_t	=	thickness relaxed indicator function
χ_V	=	volume relaxed indicator function
x	=	element of $\mathbb{R}^n$ defining a point in the problem domain
x	=	generic design point
x_i^{old}	=	random search design point component
x_i^{try}	=	random search tentative design point component
x_l	=	local spanwise coordinate
y	=	spanwise coordinate
y_l	=	local chordwise coodinate
$\mathbb{Z}$	=	space of integers
z	=	thickness direction coordinate
$\partial\alpha^r/\partial\delta$	=	rigid wing twist resulting from a unit aileron deflection
β	=	wing twist
δ	=	aileron deflection
ϵ	=	smoothing domain dimension
η	=	integration variable in the spanwise direction
θ	=	element of $[0, 2\pi]^n$
ψ	=	level set function
$\hat{\psi}$	=	Fourier coefficient
ψ_ϵ	=	smoothed ψ
ψ_ϵ^N	=	finite Fourier expansion of ψ_ϵ

Presented as Paper 4608 at the 10th AIAA/ISSMO Multidisciplinary Analysis and Optimization Conference, Palm Springs, CA, 19–22 April 2004; received 6 February 2006; revision received 16 March 2007; accepted for publication 23 April 2007.

*Assistant Professor, Department of Mechanical Engineering, Avenida Rovisco Pais.

†Professor, Department of Mechanical Engineering, University of Victoria, P.O. Box 3055, Victoria, BC, V8W 3P6, Canada. Associate Fellow AIAA.

I. Introduction

IN THIS study, we consider the optimization of the reinforcement layout of a wing box to enhance its roll maneuverability. The problem is formulated using a framework for topology optimization based on the spectral level set approach.

We address roll performance in terms of aileron reversal. The principle behind control surface reversal [1] can be described in a simple two-dimensional setting: consider an airfoil equipped with an aileron deflected downwards to provide additional lift. The flow acting on the aileron generates a moment of force that twists the airfoil nose down, thus reducing the angle of attack and the aileron incidence. Consequently, the net lift generation is decreased and, for the same aileron deflection, the rolling moment for an elastic wing is less than that for a rigid wing. This loss of aileron effectiveness is a consequence of the elastic properties of the wing and is dependent on the flight condition. If not accounted for, this condition can lead to a reduction of the vehicle's performance in roll maneuvers.

Previously, the standard way of dealing with the decrease in aircraft performance due to problems concerning control effectiveness and reversal was to avoid, as much as possible, the flexibility of the wing. This approach resulted in a stiffened wing and therefore an increase in the aircraft structural weight.

The Mission Adaptive Wing (MAW) [2] and the Active Flexible Wing [3] programs, in the 1980s, were turning points with respect to roll maneuvering efficiency. Both programs challenged the conventional control surface design practice, without the weight penalty, through the development of morphing aircraft. Aeroelastic deformations were also exploited in a beneficial manner in the Active Aeroelastic Aeronautic Structures European program and in the Smart Wing program [4].

However, applications of those benefits have failed to be introduced in commercial air vehicles. Also, the actuation technology for the implementation of the innovative concepts has fallen short of expectations. For example, actuator systems lacked the energy and weight requirements to make the MAW program viable practical technology. Moreover, the integration of the actuators into the wing structure added complexity to the program's drawbacks. Also, in the 1990s, the performance of a hingeless smart memory alloy based control surface in the Smart Wing program was limited by the alloy's actuation bandwidth and range.

In recent years, material science and engineering have witnessed considerable new developments in composite materials. It is therefore viable to readdress the idea of reinforcing a wing with the perspective of producing an optimized stiff, but also light, wing for roll maneuvering enhancement.

The determination of the optimal topology of the reinforcement layout of a structure is a natural extension of structural topology optimization design, in which the optimizer searches for minimizing configurations among topologically distinct classes. Consequently, in structural optimization for instance, holes may appear or disappear from the initial design, and breakages and merges of the structure may occur. In this way, the optimal design may have a different topology than the initial design, which implies a larger set of possible structures and thus an eventually better design than the one obtained following traditional size and shape optimizations.

The main approach to structural boundary design is the homogenization method [5–7], in which the initial design is composed of a repeated base cell made of an arrangement of solid material and void space. The design variables of the optimization problem define that arrangement. Another important approach is SIMP [8]. In this case, the stiffness is multiplied by a densitylike function with values between zero and one, which becomes the design variable of the optimization problem. Other theories include the evolutionary algorithm [9], in which solid elements are deleted from a fixed mesh to decrease the objective function, and the bubble method [10], in which holes are positioned along the structure, thus changing its initial topology.

The spectral level set methodology [11] is based on the level set methods [12]. According to these methods, the relevant boundary or interface is the zero level set of a function, that is, the sign of the level set function determines whether we are outside or inside the interface. As this function evolves during the optimization, so does the boundary. In this way, an interface can easily sustain topological changes, establishing the level set approach as an adequate tool in topology optimization problems, which, inherently, require an on–off nature. Classic level set methods use the nodal values of the level set function as the design variables of the optimization problem. The spectral level set methodology expands this function into a finite Fourier series and uses its coefficients as the design variables.

Sethian and Wiegmann [13] used the level set approach to achieve fully stressed structures. Osher and Santosa [14] and Allaire et al. [15,16] have also applied the level set methods to structural optimization.

The application of topology optimization to aeroservoelasticity is very recent, of which several studies [17–19] are good examples. In particular, Maute and Reich [19] propose the integration of mechanisms in the aeroelastic optimization of adaptive airfoils considering both aerodynamic and structural constraints and using a level set approach. In Gomes and Suleman [11], the spectral level set methodology is used to design a morphing airfoil that enhances the performance of its aileron effectiveness.

This paper is divided into two main parts: a brief description of the key ideas behind the spectral level set methodology, and the application of the proposed methodology to the design of a reinforced wing box with an improved roll maneuvering performance.

II. Spectral Level Set Methodology

The spectral level set methodology is a tool used to formulate optimization problems involving the evolution of an interface. It inherits from the level set formulation [12] the idea of embedding the evolution of an interface into the evolution of a function as its zero level set. In this way, the sign of this function determines whether we are outside or inside the interface, thus providing the methodology with an on–off character. During the optimization, the level set function evolves and so does the interface. In this way, a structural boundary can easily sustain topological changes, establishing the level set approach as an adequate tool in topology optimization problems. However, instead of defining this function using its nodal values, the spectral level set methodology uses the coefficients of its Fourier series expansion for its definition. The Fourier coefficients become the design variables of the optimization problem assigned to the interface definition.

One advantage of the proposed methodology is to reduce, under certain circumstances, the number of variables assigned to describe the interface. This topic will be considered in Sec. II.A. Another advantage of the spectral level set methodology is to avert successive mesh generation during the optimization algorithm. This property follows from the works of Xie and Steven [9] and Sethian and Wiegmann [13]. Following this reasoning, a fixed discretization mesh is imposed on the domain of the level set function.

Another advantage of the spectral level set approach in structural topology optimization is to intrinsically avoid the development of checkerboardlike patterns in the optimal design, corresponding to a sequence of alternating solid and void mesh elements [20].

Contrary to traditional level set methods approaches, the proposed formulation does not consider the level set function to be a solution of a Hamilton–Jacobi equation. As a result, the spectral level set methodology is able to nucleate new holes in the interior of the interface in a two-dimensional setting. Therefore, the formation of new holes is possible. In this way, the design space is larger in the sense that it includes layouts that are topologically different from the initial layout. Consequently, the solution found by the optimization algorithm is better than or equal to the solution corresponding to a smaller design space. Other solutions to avoid the lack of nucleation mechanism have been addressed in Sokolowski and Zochowski [21] and Allaire et al. [22].

Here we present the error estimates involved in the spectral level set methodology. A detailed description is found in Gomes and Suleman [11]. Let $\psi : [0, 2\pi]^n \to \mathbb{R}$ be the level set function. The Fourier coefficients of ψ are

$$\hat{\psi}(k) = \frac{1}{(2\pi)^n} \int_{[0,2\pi]^n} \psi(\theta) e^{-ik\cdot\theta} \, \mathrm{d}\theta \tag{1}$$

for ψ defined as a function of $\theta \in [0, 2\pi]^n$. The Fourier inversion formula is given by

$$\psi(\theta) = \sum_{k\in\mathbb{Z}^n} \hat{\psi}(k) e^{ik\cdot\theta} \tag{2}$$

In general, we wish to identify $[0, 2\pi]^n$ with the physical space defined by the variable $x \in \mathbb{R}^n$. Assume $x \in [a_1, b_1] \times \cdots \times [a_n, b_n]$. Then, each component of θ is linearly related to the corresponding component of x through $\theta_i = \frac{2\pi}{p_i}(x_i - a_i)$, in which $p_i = b_i - a_i$ is the period corresponding to coordinate $i = 1, \ldots, n$.

A. Error Estimates

Consider the set of functions constructed from a finite Fourier series. A key question in the spectral level set methodology, addressed in this section, consists of estimating the error of this approximation of the level set function.

The existence of an infinite number of functions with the same zero level set implies the lack of uniqueness of the level set function in the description of an interface. In this study, we choose one of these functions and then analyze if its zero level set can be adequately represented by the zero level set of a finite Fourier expansion.

In this work, we consider the signed distance to the interface as our level set function. It is a Lipschitz continuous function for any degree of regularity of the interface. Therefore, it can be uniformly approximated by the Fourier series. However, results from the theory of the Fourier series [23] determine that the regularity of the signed distance to the interface should be increased to guarantee the convergence of its Fourier series. To this end, we proceed with the smoothing of the signed distance to the interface.

B. Smoothing

The smoothing, or mollification [24], results in a smooth function very similar to the original except at sharp corners. At these points, the original function undergoes an averaging operation. An upper bound for the error committed in the smoothing procedure, that is, the difference between the original, ψ, and the smoothed, ψ_ϵ, level set functions can be found in Gomes and Suleman [11] to be

$$|\psi_\epsilon(x) - \psi(x)| \leq C\epsilon \tag{3}$$

in which $C > 0$ is a constant. From Eq. (3), we conclude the smoothing error is controlled linearly by the factor ϵ, which is a measure of the n-dimensional ball we need to smooth ψ out, and therefore it depends on the degree of smoothness of ψ.

C. Truncation Error

Suppose the finite Fourier expansion of ψ_ϵ, ψ_ϵ^N includes only the terms with $k \in \mathbb{Z}^n$ such that the components of k lie on a cube of side $2N$ centered at the origin. The square radius $N \in \mathbb{N}$ determines the number of Fourier modes included in the series expansion. Given the smoothed signed distance to the interface, an estimate of the error committed in using a finite Fourier series expansion is also provided in Gomes and Suleman [11] as

$$\|\psi_\epsilon(\theta) - \psi_\epsilon^N(\theta)\|_\infty \leq \frac{C}{\epsilon^m N^{m-n}}, \qquad m > n \tag{4}$$

in which m is an arbitrarily large parameter.

D. Total Error Bound

The total error bound involved in the proposed methodology, which is the sum of the smoothing and truncation error bounds, is

$$\|\psi(\theta) - \psi_\epsilon^N(\theta)\|_\infty \leq \frac{C}{N^{\frac{m-n}{m+1}}}, \qquad m > n \tag{5}$$

that is, asymptotically proportional to $1/N$, as $m \to \infty$. This means that it is possible to construct at least one level set function, the smoothed signed distance function, whose zero level set function approximates any given interface. Moreover, we can approximate this function with a finite Fourier series to any desired accuracy. Note that this estimate is asymptotically independent of n, which implies our method should be almost as fast in three-dimensional problems as in two-dimensional problems.

This error is of the same order as the one in classic nonadaptive spacial discretizations of ψ considering N nodes. However, if the level set function is sufficiently smooth, we can prove asymptotically in N, that the proposed methodology achieves the same error with less design variables than spacial discretizations [11]. That is, under certain circumstances, the spectral level set methodology could lead to the reduction of the design space dimension.

The reduction of the number of variables used to describe an interface is particularly useful in multidisciplinary optimization design problems. In fact, a desirable feature in these complex problems is to achieve optimal designs in an expeditious fashion. One way to pursue this goal is to describe, for example, a structural boundary using a small number of design variables. Therefore, in certain cases, the spectral level set methodology is expected to enhance the performance of multidisciplinary design tools.

The choice of the signed distance function for our level set function was arbitrary. In fact, there may be other functions that represent the same interface and are better approximated by a truncated Fourier series. This means our method may perform considerably better than the predicted error bounds.

III. Reinforced Wing Box

In this section, we determine the reinforcement layout of a wing torsion box for increased aircraft roll maneuverability under the framework of the spectral level set methodology. One way to improve the roll performance of the aircraft is to maximize the aileron reversal dynamic pressure. This corresponds to maximize the speed at which the aileron ceases to provide additional lift. We initialize the optimization problem with configurations belonging to different topology classes.

A. Background

Aileron reversal [1] can be simply stated as follows. Consider a wing equipped with an aileron deflected downwards to provide additional lift. The flow acting on the aileron generates a moment of force that twists the wing nose down, thus reducing the angle of attack and the aileron incidence. Consequently, the net lift generation is decreased and, for the same aileron deflection, the rolling moment for an elastic wing is less than that for a rigid wing. This loss of aileron effectiveness is a consequence of the elastic properties of the wing and is dependent on the flight condition. If not accounted for, this condition can lead to a reduction of the vehicle's performance in roll maneuvers. In a case in which the aileron produces no lift, we say the aileron has reversed. The dynamic pressure at which this occurs is the aileron reversal dynamic pressure.

Suppose a straight wing is subject to an antisymmetrical lift distribution resulting from differential aileron deflections. Consider the following system of coordinates. The x axis points to the aircraft's rear and is defined along the root of the half wing; the y axis starts at the root of the half wing, points to its tip, and is defined along the wing's elastic axis. Figure 1 shows this system of coordinates.

Consider the following assumptions:

1) All of the local force coefficients are applied at the aerodynamic center of each station.

2) The rolling acceleration is zero.

3) The twist distribution along the wing is a linear function of the aileron deflection and of the attack angle induced by the rolling velocity.

4) The line of aerodynamic centers coincides with the elastic axis of the wing.

5) The chord c and the local two-dimensional slope of the lift curve, a_0, are constant along the wing span.

Finally, assume strip theory. An expression for the aileron reversal dynamic pressure, q_R, of a straight wing based upon the stated simplifying assumptions is

$$q_R = -\frac{C_{l_\delta}}{\frac{1}{Sl}\int_0^l a_0 \int_{l_1}^{l_2} C^{\theta\theta}(y,\eta)\frac{\partial c_{mAC}}{\partial \delta} c^2 \,\mathrm{d}\eta c y \,\mathrm{d}y} \tag{6}$$

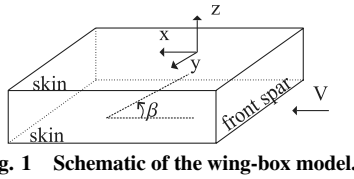

Fig. 1 Schematic of the wing-box model.

where C_{l_δ} is the derivative of the rolling moment coefficient of the rigid airplane with respect to the aileron deflection δ, given by

$$C_{l_\delta} = \frac{1}{Sl}\int_{l_1}^{l_2} a_0 \frac{\partial \alpha^r}{\partial \delta} c y \, \mathrm{d}y \tag{7}$$

where S is the planform area of the wing; l is the half the wing span; $y \in [l_1, l_2]$ is the portion of the wing having the aileron; $\partial\alpha^r/\partial\delta$ is the twist of the rigid wing resulting from a unit aileron displacement; the influence function $C^{\theta\theta}(y, \eta)$ is the twist at y produced by a unit moment, with the same direction as the twist, at η; and c_{mAC} is the local moment coefficient. The dynamic pressure in Eq. (6) corresponds to a speed at which the lift increment due to δ is zero. An increment in the deflection of the aileron would result in a negative lift.

In light of the aforementioned assumptions, Eq. (7) can be written in another fashion. The assumption of strip theory implies $\partial c_{mAC}/\partial\delta$ is nonzero only on the portion of the wing having the aileron. In this particular case, the twist distribution β along the span is given as

$$\beta(y) = q\delta \int_{l_1}^{l_2} C^{\theta\theta}(y, \eta) \frac{\partial c_{mAC}}{\partial \delta} c^2 \, \mathrm{d}\eta \tag{8}$$

which in turn implies

$$q_R^2 = -\frac{C_{l_\delta}}{\frac{1}{Sl}\int_0^l a_0 \beta(y) c y \, \mathrm{d}y} \tag{9}$$

for a unit aileron deflection. In Eq. (8), q stands for dynamic pressure.

B. Wing-Box Model

In this application, we want to maximize q_R^2 as in Eq. (9), which depends on the wing's internal structure through $C^{\theta\theta}$. In a preliminary analysis, the resistance to axial and bending loads is carried by the wing skin and its stringers, whereas torsional and shear loads are supported by the shear stresses developed in the wing skin and spar webs. A simple idealization of a wing subject to torsional loads for which the internal structure is perceived is a wing-box model composed of two spars and upper and lower skins between two consecutive ribs. No stringers or spar flanges were added to the model. Figure 1 shows a schematic of the wing torsion box model.

To simulate rigid ribs perpendicular to the y axis, we imposed suitable boundary conditions to the wing-box model [25]. The four components, two spars and two skin sections, were modeled as four plates fixed at $y = 0.0$ m. At the opposite end, that is, at $y = l$, the rotations about the two axes perpendicular to the span direction were set to zero. Also, we defined a rigid body as the set of all the points at $y = l$. We applied a torque to this rigid body to simulate the aerodynamic load proportional to $\partial c_{mAC}/\partial\delta$. It consists of a negative moment in the y direction of magnitude $250,000$ N · m.

The wing torsion box is 1.0 m along the span, 2.5 m along the x direction, and 0.14 m in height. Both spars have a constant thickness of 0.04 m and the lower skin has a thickness of 0.02 m. The nodes in the upper skin belonging to the front and aft spars have a constant thickness of 0.04 m and are nondesign domain.

C. Optimization Problem

Given a prescribed amount of material, our optimization problem consists of maximizing q_R, the aileron reversal dynamic pressure, through the reinforcement of the wing's upper skin. The zero level set of the level set function, ψ, defines the thickness variation over the upper skin: if the function is positive, then the thickness is maximum; if the function is negative, then the thickness is minimum. The Fourier coefficients of the level set function are the design variables of the optimization problem.

In Eq. (9), an aileron-down deflection generates a nose-down twist of the wing, which corresponds to a negative β according to Fig. 1. All the other parameters in Eq. (9) are positive. Consequently, the optimization problem can be stated as

$$\min_{\text{Fourier coeff.}} -\int_0^l \beta(y) y \, \mathrm{d}y \tag{10}$$

subject to

$$\frac{V_{\text{reinf}}(\psi)}{V_{\text{total}}} \le 0.3 \tag{11}$$

and to the elasticity problem, in which V_{reinf} is the volume of the reinforcing material and V_{total} is the volume of the original upper skin.

The twist angle β distribution along the span is the solution of the elasticity problem defined for the wing-box structure with the boundary conditions defined in Sec. III.B.

For this application, the design domain is the upper skin of the wing box. It has a minimum thickness of 0.02 m and a maximum thickness of 0.04 m.

D. Implementation

1. Initial Designs

In this application of the spectral level set methodology, we considered six initial designs. Five of the six initial layouts are depicted in Figs. 2a, 3, 7a, 8a, and 9a. The sixth initial design consists of an all-reinforced upper skin, which does not satisfy constraint Eq. (11). Except for the designs in Figs. 2a and 7a, which are in the same class, all of the other configurations belong to different topological classes.

The designs of Figs. 2a and 3 are educated guesses about the optimal configuration based on the following consideration of the physics and symmetry of the optimization problem: the boundary conditions imposed on the wing-box structure will result in a twisting distribution that increases with y. This means β achieves a maximum value at the maximum value of y. Accordingly, there are two reasonable configurations for the optimal pattern of the reinforcing material. The configuration of Fig. 2a consists of an even distribution of the maximum amount of reinforcement material along the neighborhood of the chord defined by $y = l$. In this way, the reinforced stations become stiffer and therefore the twisting of that part of the wing decreases in comparison with the nonreinforced wing box.

The other interesting configuration, depicted in Fig. 3, is a symmetric distribution of the maximum amount of reinforcement material equally between the leading and the trailing edges. With this type of reinforcing distribution, the leading and trailing edges twist less and therefore there is a chance the objective function achieves a minimum value.

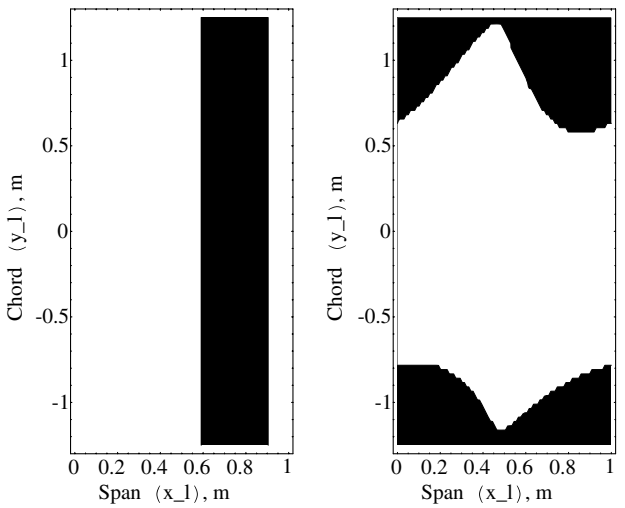

a) Initial layout **b) Optimal layout**

Fig. 2 Design of the initially reinforced tip.

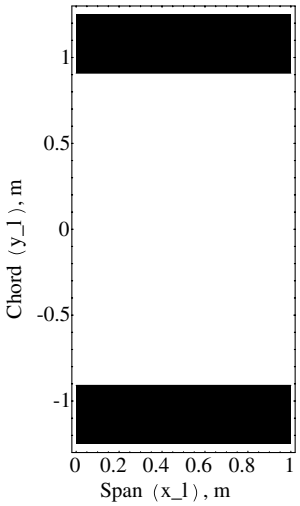

Fig. 3 Initial layout of reinforced leading and trailing edges.

2. Relaxation

The level set function ψ integrates optimization problems through a relaxed indicator function. In this case, the relaxed formulation affects the computation of the objective function and the determination of V_{reinf}.

To compute the objective function, in particular, the twist angle distribution over the wing's span, we need to know the layout of the reinforcements over the upper skin. Its thickness is given by

$$\chi_t(\psi) = [\arctan(a_t\psi)/\pi + 1.5]b_t \tag{12}$$

where a_t regulates the smoothness of the indicator function and b_t is the minimum thickness value.

The determination of V_{reinf} is also subjected to a relaxed approach, thus converting the constraint Eq. (11) into a smooth function of ψ. The relaxed indicator function

$$\chi_V(\psi) = \arctan(a_V\psi)/\pi + 0.5 \tag{13}$$

constitutes the integrand of the quadrature integral used to compute V_{reinf}.

The values chosen for parameters a_t and a_V depend on the physics of the problem and on the optimization algorithm. Typically, it is necessary to proceed with the tuning of these values during simulation.

3. Elasticity Solver and Finite Element Mesh

The elasticity problem solver used for computing the twist angle β was ABAQUS/Standard 6.3© [26].

The wing-box model is composed of four plates: two 2.5×1.0 m plates for the upper and lower skins, and two 1.0×0.14 m for the front and rear spars. The finite element mesh for each skin is composed of 250 square 0.1×0.1 m elements. Each spar grid has 40 rectangular 0.1×0.035 m elements.

The plates are discretized using thick shell elements S8R from the ABAQUS/Standard 6.3© library. This is a reduced integration eight-node element whose nodal thickness option allows thickness variation over the element. There are 6 degrees of freedom at each node: three displacements along the three coordinate axes and three rotations about those axes.

4. Integration Quadratures

The integration quadrature for the objective function is the trapezoidal rule. To compute the volume of the reinforcements, we use a nine-node Newton–Cotes quadrature, in which the value of ψ at the element middle point is interpolated from ψ at the other eight nodes.

5. Optimization

The optimization algorithm is composed of two steps: a quick random search [11] of the design space followed by a local search with COBYLA [11], a derivative-free optimization tool.

The objective function considered during the random search procedure is constructed from the integral objective function in Eq. (10) and $g(x) = V_{\text{reinf}}[\psi(x)] - 0.3V_{\text{total}}$ as

$$f(x) = \tilde{f}(x) + \text{PEN}\max\{0.0, g(x)\} \tag{14}$$

where PEN is a positive user-defined constant chosen at the beginning of the random search module. Also chosen is MAXTRIES, which regulates the termination schedule by specifying the maximum number of calls to the module calculating $\tilde{f}$ and g. Here, x represents an array of design variables, which in the case of the proposed methodology are the Fourier coefficients of ψ. At each step, x are pseudorandom numbers chosen from a uniform distribution in the range $[-0.5, 0.5[$, according to

$$x_i^{\text{try}} = x_i^{\text{old}} + \text{FACTOR}[\text{RAND}() - 0.5] \tag{16}$$

where $i = 1, 2, \ldots, n$ stands for the component of x, the constant FACTOR is used to scale the added random number to the order of magnitude of x^{old}, and RAND() is a FORTRAN function returning a real pseudorandom number from the uniform distribution in the range $[0.0, 1.0[$. The set x^{try} is accepted if $f(x_{\text{try}}) < f(x_{\text{old}})$. The random search terminates once MAXTRIES x_{try} have been generated.

Our main optimization tool is COBYLA, a trust region method for constrained minimization without derivatives described in Powell [27]. No a priori conditions are assumed concerning the degree of regularity of f and g and the type of relation, linear or nonlinear, between these and x. The user must set the number of design variables, the number of inequality constraints, and the parameters RHOBEG and RHOEND, which define the size of the trust region. The user also assigns an integer to the variable MAXFUN, which limits the number of calls to calculate the objective and constraint functions and provides the initial vector of design variables. The output from COBYLA shows parameter MAXCV, which returns the maximum constraint violation. The values of the parameters regulating the random search and COBYLA, which were tuned for this particular problem during testing, are displayed in Table 1.

6. β Computation

At each wing station y, the twist angle $\beta(y)$ was computed using the displacement in the z direction of the nodes in the front and aft spars defined at $z = 0$ m. Given one pair of corresponding spar nodes, we calculate the average of the absolute value of the z displacement and denote it as $|z|_{\text{av}}$. These displacements have opposite signs because we are applying a torsional moment to the wing box.

Table 1 Optimization parameters

Random		COBYLA	
MAXRIES	500	RHOBEG	0.5
PENALTY	1000.	RHOEND	1.E − 05
FACTOR	0.1	MAXFUN	40,000

Table 2 Quantitative results for initially reinforced tip

	J, 10^{-7} m^2	MAXCV, 10^{-7} m^3
Initial	424.450	773,288.0
$a_t = a_V = 100.0$	375.835	2.68221
$a_t = a_V = 1000.0$	375.466	4.47035
$a_t = a_V = 10,000.0$	375.428	2.08616

Table 3 Quantitative results for initially reinforced leading and trailing edges

	$a_t = a_V = 100.0$		$a_t = a_V = 1000.0$		$a_t = a_V = 10,000.0$	
	J, 10^{-7} m^2	MAXCV, 10^{-8} m^3	J, 10^{-7} m^2	MAXCV, 10^{-8} m^3	J, 10^{-7} m^2	MAXCV, m^3
Initial	378.235	0.0	378.428	0.0	378.451	0.0
$N = 3$	374.328	205.636	373.285	68.5453	373.706	0.0
$N = 2$	373.930	8.94070	373.778	26.8221	373.633	0.0
$N = 1$	374.222	80.4663	377.018	2.98023	374.750	0.0

The magnitude of the twist β is calculated by dividing $|z|_{\text{av}}$ by half the station chord. This yields $\tan(\beta)$, which for small β, as is the case, approximates β quite well. The sign of the twist is given accordingly to the sign of the load acting on the wing box. In this case, β is negative.

E. Results and Discussion

Except for the all-reinforced upper skin initial condition, the optimization algorithm did not include the random search of the design space. The value of the objective function at the obtained minimizer is denoted by J and the constraint violation at that point is MAXCV. All the graphics in this section are referred to a local coordinate system with coordinates x_l along the span and y_l along the chord, corresponding to y and $-x$, respectively.

Figure 2b depicts the optimal design for $N = 1$, corresponding to five Fourier coefficients and nine design variables, with the initial configuration of Fig. 2a. This layout was obtained with an iterative approach on parameters a_t and a_V: Figure 2a was the initial design for COBYLA with $a_t = a_V = 100.0$ whose result was introduced in COBYLA with $a_t = a_V = 1000.0$ and, finally, the resulting coefficients were the initial variables to COBYLA with $a_t = a_V = 10,000.0$. Table 2 shows the quantitative results for these simulations.

Next, we considered the initial design of Fig. 3. Figures 4–6 show the optimal reinforcement configurations for $N = 1$, 2, 3 with $a_t = a_V = 100.0$, $a_t = a_V = 1000.0$, and $a_t = a_V = 10,000.0$, respectively. Table 3 show the quantitative results for those simulations.

Consider the reinforcement layout of Fig. 7a, corresponding to an initially reinforced leading edge. Figure 7b displays the optimal solution obtained for $N = 1$ following an iterative approach on parameters a_t and a_V: first, 100.0; then, 1000.0; and finally, 10,000.0. Table 4 shows the quantitative results of those simulations.

Suppose the crosslike layout of Fig. 8a is the initial configuration. Figure 8b depicts the optimal solution obtained after an iterative procedure in parameters a_t and a_V, running from 100.0 to 10000.0 for $N = 1$. Table 5 displays the corresponding quantitative results.

Table 4 Quantitative results for initially reinforced leading edge

	J, 10^{-7} m^2	MAXCV, 10^{-2} m^3
Initial	434.445	6.44396
$a_t = a_V = 100.0$	376.856	0.0
$a_t = a_V = 1000.0$	374.954	0.0
$a_t = a_V = 10,000.0$	373.569	0.0

Figure 9a displays a three-diagonal-stripe initial layout, and Fig. 9b shows the corresponding optimal configuration, which was obtained for $N = 2$ and an iterative process in parameters a_t and a_V, running from 100.0 to 1000.0, with two consecutive simulations with $a_t = a_V = 1000.0$. Table 6 provides an account of the respective quantitative results.

Finally, we consider the all-reinforced upper skin as an initial configuration. The results for $N = 1$, $a_t = a_V = 1000.0$ and FACTOR = 1.0 as a random search parameter are displayed in Fig. 10 and Table 7.

In view of the optimal designs obtained from initial configurations belonging to different topological classes, we can conclude that the proposed methodology successfully yielded the same reinforcement configuration in all cases. Moreover, in all but one case, the results were attained with $N = 1$, that is, with nine design variables. For the exceptional case, it was necessary to use $N = 2$ to describe the initial pattern of diagonal stripes. However, in all of the simulations, the designer had to work his way through an iterative approach on parameters a_t and a_V. Nevertheless, the results show that in this particular example of the reinforced wing box the spectral level set methodology provided optimal layouts that are fairly independent of the initial design and has done so using a very small number of design variables.

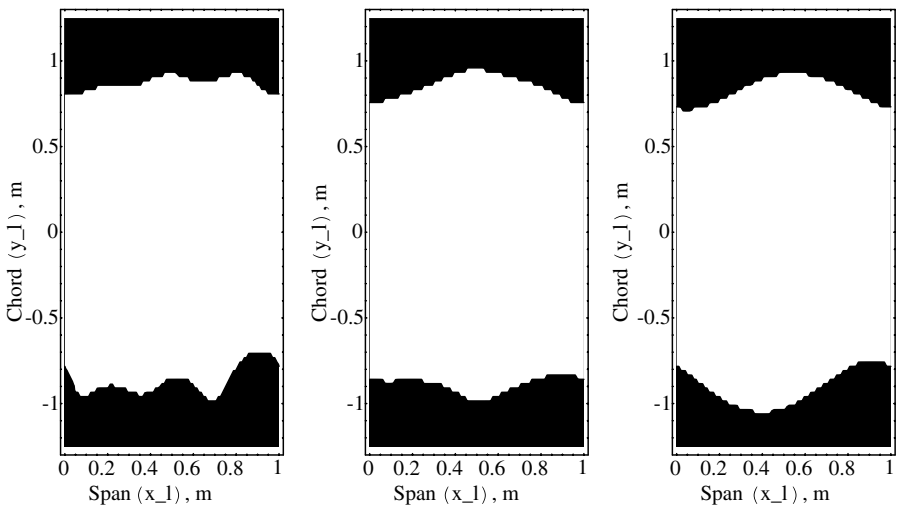

a) N=3 **b) N=2** **c) N=1**

Fig. 4 Optimal layouts for initially reinforced leading and trailing edges; $a_t = a_V = 100.0$.

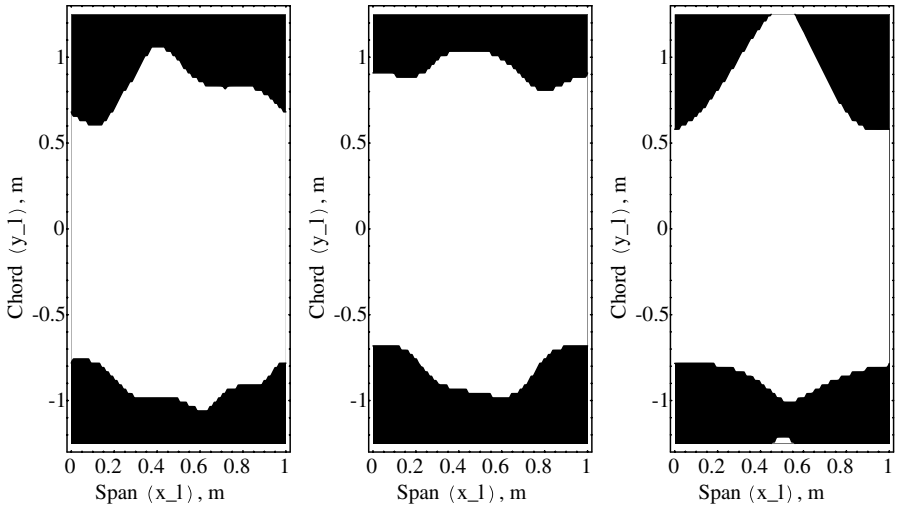

a) N=3 b) N=2 c) N=1

Fig. 5 Optimal layouts for initially reinforced leading and trailing edges; $a_t = a_V = 1000.0$.

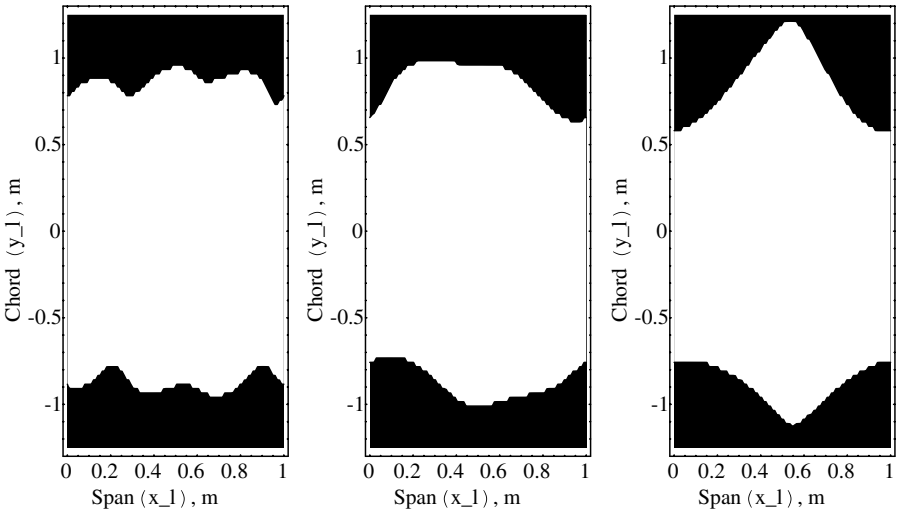

a) N=3 b) N=2 c) N=1

Fig. 6 Optimal layouts for initially reinforced leading and trailing edges; $a_t = a_V = 10,000.0$.

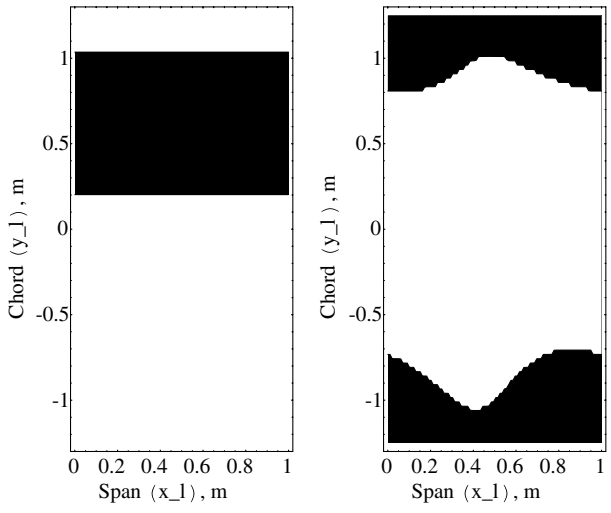

a) Initial layout b) Optimal layout

Fig. 7 Design for the initially reinforced leading edge.

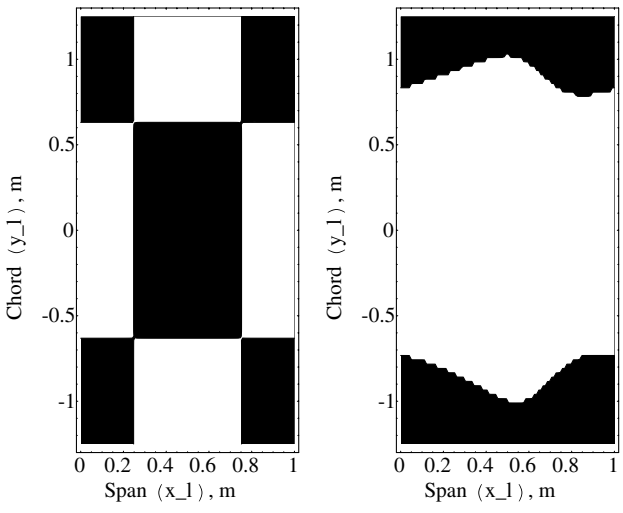

a) Initial layout b) Optimal layout

Fig. 8 Design for the crosslike initial pattern.

Table 5 Quantitative results for crosslike initial pattern

	J, 10^{-7} m^2	MAXCV, 10^{-7} m^3
Initial	395.972	5,000,010.0
$a_t = a_V = 100.0$	373.867	11.6229
$a_t = a_V = 1000.0$	373.561	6.25849
$a_t = a_V = 10,000.0$	373.528	11.6229

Table 6 Quantitative results for diagonal stripes initial pattern

	J, 10^{-7} m^2	MAXCV, 10^{-7} m^3
Iinitial	401.030	4,846,660.0
$a_t = a_V = 100.0$	385.621	12.2190
$a_t = a_V = 1000.0$	374.308	2.08616

Table 7 Quantitative results for all-reinforced upper skin initial layout

	J, 10^{-7} m^2	MAXCV, 10^{-7} m^3
Initial	2110.59	——
Initial (no penalty included)	361.375	——
$a_t = a_V = 1000.0$	374.141	9.23872

IV. Conclusions

In this paper, the spectral level set methodology is used to formulate the optimal design of a reinforced wing structure for increased aircraft roll maneuverability. To this end, the aileron reversal speed is maximized by applying a limited amount of reinforcing material to the upper skin of a wing torsion box.

The spectral level set methodology successfully attained the same optimal design for initial configurations belonging to different topology classes. According to the applied approach, the boundary defining the reinforcement layout is an interface, whose propagation, during the optimization procedure, is embedded in the evolution of the level set function as its zero level set. Also, the discretization of the level set function considers the coefficients of its Fourier series expansion. These coefficients become the design variables assigned to the description of the interface within the topology optimization problem.

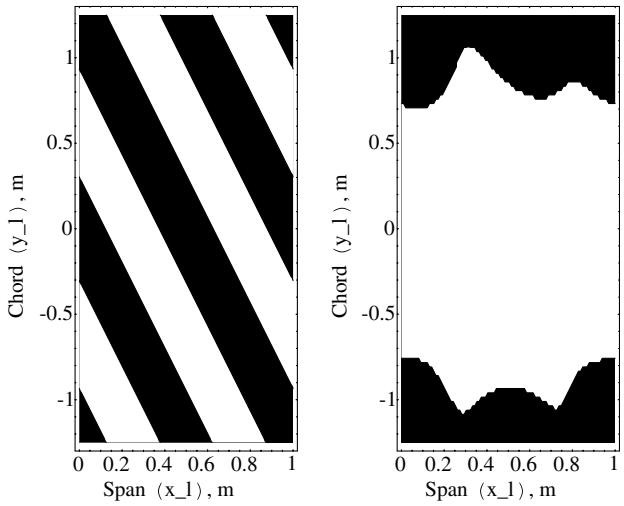

a) Initial layout **b) Optimal layout**

Fig. 9 Optimal design for the initial pattern of diagonal stripes.

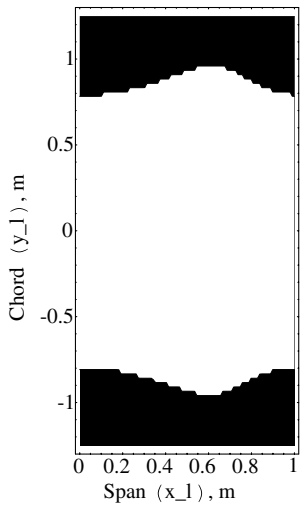

Fig. 10 Wing box: optimal design for the all-reinforced upper skin initial layout.

Our aim was twofold. On the one hand, we want to put forward a new tool to formulate topology optimization problems, the spectral level set methodology, which potentially provides the ability to describe an interface with a small number of degrees of freedom, resulting in a reduction of the design space dimension. This is particularly useful in multidisciplinary optimization settings. On the other hand, we wish to readdress the idea of stiffened aircraft structures using advanced composite materials.

Acknowledgments

The authors are grateful for the financial support of Fundação para a Ciência e a Tecnologia, Programa PRAXIS XXI and of the European Social Fund under Community Support Framework III and the POCTI-EME-61587-2004 project.

References

[1] Bisplinghoff, R. L., Ashley, H., and Halfman, R. L., *Aeroelasticity*, Dover, New York, 1996.

[2] Hall, J., "Executive Summary AFTI/F-111 Mission Adaptive Wing," Wright Research Development Center, Rept. WRDC-TR-89-2083, Wright–Patterson Air Force Base, OH, Sept. 1989.

[3] Miller, G. D., "Active Flexible Wing (AFW) Technology," Air Force Wright Aeronautical Lab, Rept. AFWAL-TR-87-3096, Dayton, OH, Feb. 1988.

[4] Kudva, J., Martin, C., Scherer, L., Jardine, A., McGowan, A.-M., Lake, R., Sendeckyj, G., and Sanders, B., "Overview of the DARPA/AFRL/NASA Smart Wing Program," *Smart Structures and Materials 1999: Industrial and Commercial Applications of Smart Structures Technologies*, Vol. 3674, Society of Photo-Optical Instrumentation Engineers, Bellingham, WA, March 1999, pp. 230–236.

[5] Bendsøe, M., and Kikuchi, N., "Generating Optimal Topologies in Structural Design Using a Homogenization Method," *Computer Methods in Applied Mechanics and Engineering*, Vol. 71, No. 2, Nov. 1988, pp. 197–224. doi:10.1016/0045-7825(88)90086-2

[6] Bendsøe, M., Diaz, A., and Kikuchi, N., "Topology and Generalized Layout Optimization of Elastic Structures," *Topology Design of Structures*, edited by M. P. Bendsoe and C. A. Mota-Soares, Vol. 227, NATO ASI Series, Series E, Kluwer, Dordrecht, 1993, pp. 159–205.

[7] Bendsøe, M., *Optimization of Structural Topology, Shape and Material*, Springer–Verlag, Berlin, 1995.

[8] Rozvany, G. I. N., and Zhou, M., "Applications of the COC Algorithm in Layout Optimization," *Engineering Optimization in Design Processes*, edited by C. M. H. Eschenauer and N. Olhoff, Springer–Verlag, Berlin, 1991, pp. 59–70.

[9] Xie, Y., and Steven, G., *Evolutionary Structural Optimization*, Springer–Verlag, New York, 1997.

[10] Eschenauer, H., Kobelev, V., and Schumacher, A., "Bubble Method for Topology and Shape Optimization of Structures," *Structural Optimization*, Vol. 8, No. 1, Aug. 1994, pp. 42–51. doi:10.1007/BF01742933

[11] Gomes, A. A., and Suleman, A., "Application of the Spectral Level Set Methodology in Topology Optimization," *Structural and Multidisciplinary Optimization*, Vol. 31, No. 6, June 2006, pp. 430–443. doi:10.1007/s00158-006-0005-2

[12] Osher, S., and Sethian, J., "Fronts Propagating with Curvature Dependent Speed: Algorithms Based on the Hamilton–Jacobi Formulation," *Journal of Computational Physics*, Vol. 79, No. 1, Nov. 1988, pp. 12–49. doi:10.1016/0021-9991(88)90002-2

[13] Sethian, J., and Wiegmann, A., "Structural Boundary Design via Level Set and Immersed Interface Methods," *Journal of Computational Physics*, Vol. 163, No. 2, Sept. 2000, pp. 489–528. doi:10.1006/jcph.2000.6581

[14] Osher, S., and Santosa, F., "Level Set Methods for Optimization Problems Involving Geometry and Constraints 1. Frequencies of a Two-Density Inhomogeneous Drum," *Journal of Computational Physics*, Vol. 171, No. 1, July 2001, pp. 272–288. doi:10.1006/jcph.2001.6789

[15] Allaire, G., Jouve, F., and Toader, A.-M., "A Level-Set Method for Shape Optimization," *Comptes Rendus Mathematique*, Vol. 334, No. 12, 2002, pp. 1125–1130. doi:10.1016/S1631-073X(02)02412-3

[16] Allaire, G., Jouve, F., and Toader, A.-M., "Structural Optimization Using Sensitivity Analysis and a Level Set Method," *Journal of Computational Physics*, Vol. 194, No. 1, 2004, pp. 363–393. doi:10.1016/j.jcp.2003.09.032

[17] Maute, K., Nikbay, M., and Farhat, C., "Conceptual Layout of Aeroelastic Wing Structures by Topology Optimization," AIAA Paper 2002-1480, April 2002.

[18] Maute, K., and Allen, M., "Conceptual Design of Aeroelastic Structures by Topology Optimization," *Structural and Multidisciplinary Optimization*, Vol. 27, Nos. 1–2, May 2004, pp. 27–42. doi:10.1007/s00158-003-0362-z

[19] Maute, K., and Reich, G., "An Aeroelastic Topology Optimization Approach for Adaptive Wing Design," AIAA Paper 2004-1805, April 2004.

[20] Sigmund, O., and Petersson, J., "Numerical Instabilities in Topology Optimization: A Survey on Procedures Dealing with Checkerboards, Mesh-Dependencies and Local Minima," *Structural Optimization*, Vol. 16, No. 1, Aug. 1998, pp. 68–75. doi:10.1007/BF01214002

[21] Sokolowski, J., and Zochowski, A., "On the Topological Derivative in Shape Optimization," *SIAM Journal on Control and Optimization*, Vol. 37, No. 4, 1999, pp. 1251–1272. doi:10.1137/S0363012997323230

[22] Allaire, G., Gournay, F. D., Jouve, F., and Toader, A.-M., "Structural Optimization Using Topological and Shape Sensitivity via a Level Set Method," *Control and Cybernetics*, Vol. 34, No. 1, 2005, pp. 59–80.

[23] Taylor, M. E., *Partial Differential Equations I - Basic Theory*, Springer–Verlag, New York, 1997, Chap. 3.

[24] Evans, L. C., *Partial Differential Equations*, Vol. 19, Graduate Studies in Mathematics, American Mathematical Society, Providence, RI, 1998.

[25] Skrna-Jakl, I., Stiftinger, M., and Rammerstorfer, F., "Numerical Investigations of an Imperfect Stringer-Stiffened Composite Wing Torsion Box—An Analysis Concept," *Composites Part B: Engineering*, Vol. 27, No. 1, 1996, pp. 59–69. doi:10.1016/1359-8368(95)00007-0

[26] ABAQUS/Standard User's Manual, Ver. 6.3 , Hibbitt, Karlsson & Sorensen, Inc., Pawtucket, RI, 2002.

[27] Powell, M., "On Trust Region Methods for Unconstrained Minimization Without Derivatives," *Mathematical Programming*, Vol. 97, No. 3, Aug. 2003, pp. 605–623. doi:10.1007/s10107-003-0430-6

A. Messac
Associate Editor